Eur. Phys. J. C (2023) 83:409
https://doi.org/10.1140/epjc/s10052-023-11520-z

THE EUROPEAN PHYSICAL JOURNAL C

Regular Article - Theoretical Physics

Is it possible to distinguish between different black hole solutions using the Shapiro time delay?

Ednaldo L. B. Junior[1,a], **Manuel E. Rodrigues**[2,3,b], **Henrique A. Vieira**[2,c]

[1] Faculdade de Engenharia da Computação, Universidade Federal do Pará, Campus Universitário de Tucuruí, Tucuruí, Pará CEP: 68464-000, Brazil
[2] Faculdade de Física, Programa de Pós-Graduação em Física, Universidade Federal do Pará, Belém, Pará 66075-110, Brazil
[3] Faculdade de Ciências Exatas e Tecnologia, Universidade Federal do Pará Campus Universitário de Abaetetuba, Abaetetuba, Pará 68440-000, Brazil

Received: 21 February 2023 / Accepted: 16 April 2023 / Published online: 16 May 2023

Abstract In this paper we propose to use the Shapiro time delay as a tool to distinguish between different black hole solutions. We calculate the analytic Shapiro time using first order expansions for four solutions. These are Schwarzschild, Reissner–Nordström, Bardeen, and Ayón-Beato and García. We created a numerical experiment based on measurements in the solar system consisting of the outward and return paths of light traversing a black hole at the center. We obtained different delay times on the order of 10^{-4} s and 10^{-6} s for a stellar black hole; and variations on the order of hours for a supermassive hole. Considering that the accuracies currently achieved in solar system measurements are on the order of 10^{-12} s, we believe that this mechanism could be used in the determination of black hole models in the near future.

1 Introduction

In 1916, Schwarzschild [1] solved Einstein's new equations of general relativity [2] and introduced to the world what we know today as black holes. These physical entities are defined as a region of spacetime covered by an event horizon from which not even light can escape [3]. This first exact solution of Einstein's equations, the Schwarzschild black hole, is obtained by considering only mass, there is no angular momentum and no electric charge, and can therefore be used as an approximation to describe celestial bodies with low rotation, for example the Sun or even the Earth. Of course, it is also possible to obtain more general exact solutions that take into account rotation, electric or magnetic charge, and even both together [4]. Since the 1960s, this area has received increasing attention due to the discovery of compact objects and, more recently, the first image of the shadow of a presumably supermassive black hole [5–10]. However, there is an open problem that still causes discussion among physicists: the singularity. For example, all the above solutions have a singularity in the origin.

A curvature singularity is a sudden endpoint of the geodesics, the equations describing the motion of free particles in general relativity, at which quantities such as the density of matter become infinite. There is no definitive consensus on this issue, but most scientists believe that singularities in general relativity are a mistake because it is a classical theory. In this sense, an alternative to the problem is to look for solutions to the Einstein equations that are free of singularities. The solution proposed by Bardeen [11] is the first to achieve this goal, but it lacked a plausible source of matter. Ayón-Beato and García [12] proposed the first exact regular solution in 1998, which had as its source a self-gravitating magnetic charge described by nonlinear electrodynamics [13]. Later, the same authors showed that Bardeen's solution can be described in the same way [14], and it was also realized that one can use nonlinear electrodynamics to construct a regular black hole [15]. Now there are a variety of regular Bardeen-type solutions. Some solutions have electric charge as a source [16,17], and others also have angular momentum [18,19]. In addition, the solution has been extended to alternative theories of gravity, such as the $f(r)$-theory [20,21], the $f(G)$-theory [22,23], and rainbow gravity [24]. There are also papers in the literature showing how the regularity of the model is lost when a singular solution is attached to it [25,26].

[a] e-mail: ednaldobarrosjr@gmail.com
[b] e-mail: esialg@gmail.com (corresponding author)
[c] e-mail: henriquefisica2017@gmail.com

A natural question that arises in this context of black holes is: since these bodies do not emit light, would it be possible to distinguish between different solutions? Bozza [27], who studied gravitational lensing in the strong-field limit, suggested that Very Long Baseline Interferometry (VLBI) should be able to reconstruct the coefficients of the strong-field limit and select an accurate black hole model. Comparing the Bardeen and Reissner–Nordström solutions using the absorption [28] and scattering [29] of planar massless scalar waves, the authors conclude that the behavior of both is similar, especially when high-frequency waves are considered. In parallel with this result, two papers comparing Reissner–Nordström and Ayón-Beato and García, considering the analysis of geodesics and the absorption [30] and then the scattering [31] of a massive scalar field, have suggested that it is impossible to distinguish regular black hole solutions from standard solutions. In [32] the conclusion is the same when comparing Kerr's solution with regular solutions. In contrast to this interpretation, Stuchlík and Schee [33] claim that we can distinguish between shadows produced by a Bardeen and a Reissner–Nordström black hole due to nonlinear electrodynamics. This result can be supported by [34], which shows that black holes described by different solutions do not in general produce identical shadows.

Besides the already mentioned interactions between black holes and light – absorption, scattering and shadowing – there is another interesting effect to analyze: the delay of a light signal. This phenomenon is known as the Shapiro time delay [35] and served as the fourth test of general relativity. The experiment by Shapiro's group involved measuring the time for a light signal to be sent from Earth to Venus and reflected back to Earth while these planets were at superior conjunction, that is, aligned on a straight line through the Sun. The prediction of general relativity is that the curvature caused by the mass, in this case the Sun, causes a time delay compared to the flat case. For the Earth–Venus situation, this delay should be of the order of [36]

$$\Delta t \simeq \frac{4GM_\odot}{c^3}\left[\ln\left(\frac{4D_E D_V}{R_\odot^2}\right)+1\right], \tag{1}$$

where $G = 6.67408\times10^{-11}\ \mathrm{N\,m^2/kg^2}$ is the Newton's constant of universal gravitation, $M_\odot = 1.98892\times10^{30}$ kg is the solar mass, $c = 2.99\times10^8$ m/s is the speed of light in vacuum, $D_E = 1.495978707\times10^{11}$ m is radius of Earth's orbit and $D_V = 1.08\times10^{11}$ m is radius of Venus orbit both during superior conjunction, and $R_\odot = 6.957\times10^8$ m is the solar radius. These values lead to $\Delta t = 252.282\ \mu$s and the experimentally measured by Shapiro's group was approximately 200 μs. At the time, the agreement between the theoretical prediction and the experimental value was better than 5%. Latter, the Viking mission to Mars, in 1976, achieved a better result than 1% [37]. In 2003, the Cassini spacecraft, in mission to Saturn, used Shapiro time to measure the PPN γ parameter, the prediction of general relativity is that it is unitary, and found $\gamma = 1+(2.1\pm2.3)\times10^{-5}$ [38].

The Eq. (1) is obtained by considering the Schwarzschild metric (we will show later in more detail how to obtain the Shapiro time for any metric), starting from a first-order expansion with respect to mass, and as we have already mentioned, this result agrees well with experimental measurements. However, since we know that almost everything in the universe is rotating, Dymnikova [39] obtained the time delay by considering the Kerr metric. Another way to refine the theoretical prediction is to consider higher order terms in the expansion in terms of mass [40] or to assume a velocity for the black hole [41]. Feng and Huang [42] have shown that this effect can be achieved with a purely optical approach. In 2001, Kopeikin [43] proposed an interesting use for Shapiro time. He claimed that a measurement of the time delay of light from a quasar as it passes the planet Jupiter could be used to measure the gravitational velocity c_g. His reasoning was that the velocity v of a body such as Jupiter would cause corrections in Shapiro time on the order of v/c_g, which could make the velocity of gravity different from that of light $c_g \neq c$ [44,45]. In 2002, S. M. Kopeikin and E. B. Fomalont made precise measurements of the Shapiro delay with 10^{12} s time accuracy. They claimed that the correction term is about 20% [46]. Despite the high accuracy in time measurement, Will [47] lastly pointed out that this effect does not depend on the propagation speed of gravity, but only on the speed of light. Today, there are other uses for the Shapiro time delay: it is useful in observing pulsars [48–51]; in measuring the mass of stars [52]; and it can serve as a technique for studying ultralight dark matter [53,54].

With this context in mind, we will calculate the Shapiro time delay for four solutions; Schwarzschild, Reissner–Nordström, Bardeen and Ayón-Beato and García. Then, we will propose a idealized experiment that consists in measure a round-trip travel of a light signal sent from a planet to another when they are in superior conjunction, with the central body being a black hole described by one of this solutions. We will study this situation to respond the question: is it possible to distinguish between different black hole solutions using the Shapiro time delay? This paper will be organized as follows: in Sect. 2 we will briefly review the main aspects of the four solutions that will be discussed; in Sect. 3 we will calculate the Shapiro time for any metric; in Sect. 4 we will define and calculate the impact parameter, also for any metric; in Sect. 5 we will make the comparison for two black holes with equal event horizons and similar masses; in Sect. 6 we will make the comparison by equalizing both the event horizon and the masses; and in Sect. 7 we will draw our conclusions. We will consider throughout this work the metric signature $(-,+,+,+)$. Also, we will use, unless otherwise stated, geometrized units where $G = c = 1$.

2 Black hole solutions

In this section we will show how to obtain the solutions that are used here as examples. Also, we will show some details about it's behavior, such as the event horizon and the regularity of spacetime generated by then.

2.1 Schwarzschild

Schwarzschild's black hole is an exact solution of Einstein's field equations for the vacuum. It is a static and spherically symmetric solution described by a single parameter, the mass m. In the units we consider, geometrized,it is written as follows [36]

$$ds^2 = -\left(1-\frac{2m}{r}\right)dt^2 + \left(1-\frac{2m}{r}\right)^{-1}dr^2 + r^2 d\theta^2 + r^2\sin^2\theta d\phi^2. \tag{2}$$

This solution is singular at the origin, i.e., one or more components of the Riemann tensor diverge. A simple way to check this is to analyze the Kretschmann scalar [55]

$$K = R_{\mu\nu\alpha\beta}R^{\mu\nu\alpha\beta} = \frac{48m^2}{r^6}. \tag{3}$$

From the above result we see that this scalar diverges when $r \to 0$. For $r = 2m$, the component g_{tt} is zero, and the g_{rr} diverges. This coordinate, formerly considered a singularity, is now called the event horizon. The Schwarzschild solution has only one horizon, while the other solutions we will consider have two horizons.

2.2 Reissner–Nordström

The Reissner–Nordström metric is a charged, static and spherically symmetric solution of the Einstein–Maxwell field equations given by

$$ds^2 = -\left(1-\frac{2m}{r}+\frac{q_{RN}^2}{r^2}\right)dt^2 + \left(1-\frac{2m}{r}+\frac{q_{RN}^2}{r^2}\right)^{-1}dr^2 + r^2 d\theta^2 + r^2\sin^2\theta d\phi^2. \tag{4}$$

The parameters that describe it are the electric charge q_{RN} and the ADM mass m. As we said in the introduction, this is a singular solution. We can verify this by analyzing the Kretschmann scalar

$$K = \frac{4\left(\frac{2m}{r}-\frac{q_{RN}^2}{r^2}\right)^2 + r^4\left(\frac{6q_{RN}^2}{r^4}-\frac{4m}{r^3}\right)^2 + 4r^2\left(\frac{2m}{r^2}-\frac{2q_{RN}^2}{r^3}\right)^2}{r^4}, \tag{5}$$

which diverges when $r \to 0$. This metric has up to two event horizons, which can be found by $-g_{tt} = 0$, leading to the following results

$$r_\pm = m \pm \sqrt{m^2 - q^2}. \tag{6}$$

Note that the event horizons degenerate to a single one for a charge called critical or extreme, $q_{RN}^{ext} = m$. Make the following substitutions $x = r/q_{RN}$ and $s = q_{RN}/2m$, and write the auxiliary function leads to

$$-g_{tt} = A(x,s) \equiv 1 - \frac{1}{sx} + \frac{1}{x^2}. \tag{7}$$

If we derive the above expression and equate it to zero, we find a minimum value $x_m = 2s$. If we then set $A(x_m, s) = 0$, we find the critical value $s_c = 1/2$. This auxiliary function has the same behavior as the metric function, i.e., for values of $s < s_c$ we have two event horizons, for $s = s_c$ the horizons degenerate into just one, and when $s > s_c$ there is no event horizon. We plot of the function $A(x, s)$ in Fig. 1.

2.3 Bardeen

The Bardeen regular solution is an exact, static and spherically symmetric solution of the Einstein equations minimally coupled with nonlinear electrodynamics. It is given by

$$ds^2 = -\left(1-\frac{2M(r)}{r}\right)dt^2 + \left(1-\frac{2M(r)}{r}\right)^{-1}dr^2 + r^2 d\theta^2 + r^2\sin^2\theta d\phi^2, \tag{8}$$

with

$$M(r) = \frac{2mr^3}{\left(q_{BD}^2 + r^2\right)^{3/2}}, \tag{9}$$

where $s = |q_{BD}|/2m$, q_{BD} is the magnetic charge, and m is the ADM mass. To check the spacetime singularities, we calculate the Kretschmann scalar [55]

$$K = \frac{12m^2\left(8q_{BD}^8 - 4q_{BD}^6 r^2 + 47q_{BD}^4 r^4 - 12q_{BD}^2 r^6 + 4r^8\right)}{\left(q_{BD}^2 + r^2\right)^7}, \tag{10}$$

which is everywhere. As described in the literature, the function g_{tt} can be rewritten by the substitutions $x = r/|q_{BD}|$ and $s = |q_{BD}|/2m$

$$-g_{tt} = A(x,s) \equiv 1 - \frac{x^2}{s\left(x^2+1\right)^{3/2}}. \tag{11}$$

If we derive the above expression and equate it to zero, we find a minimum value $x_m = \sqrt{2}$ independently of the value of s. Then, imposing $A(x_m, s) = 0$ we find the critical value $s_c = 2/3\sqrt{3}$. What happens is that for values of $s < s_c$ we have two event horizons, for $s = s_c$ the horizons degenerate into just one, and when $s > s_c$ there is no event horizon. The function $A(x, s)$ is shown in the Fig. 2. In terms of the magnetic charge and mass the extremization condition is

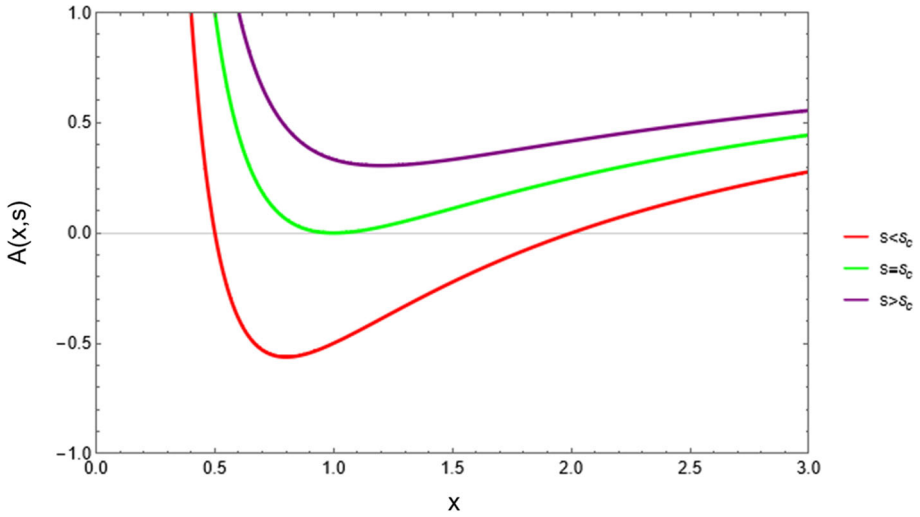

Fig. 1 Graphic representation of the auxiliary function $A(x, s)$ for Reissner–Nordström metric

$$q_{BD}^{ext} = 2ms_c = \frac{4}{3\sqrt{3}}m. \tag{12}$$

In summary, the Bardeen solution, the first regular solution, can be obtained if a self-gravitating magnetic charge is considered as the source. The action used describes nonlinear electrodynamics minimally coupled to general relativity. For more information on this black hole, see [14,28,29,56,57] and references therein.

2.4 Ayón-Beato and García

The Ayón-Beato and García regular solution is a static, and spherically symmetric solution of the Einstein equations minimally coupled to nonlinear electrodynamics, and it is the firs exact regular one. It is given by

$$ds^2 = -f(r)dt^2 + (f(r))^{-1}\,dr^2 + r^2 d\theta^2 + r^2\sin^2\theta d\phi^2, \tag{13}$$

with

$$f(r) = 1 - \frac{2mr^2}{\left(q_{ABG}^2 + r^2\right)^{3/2}} + \frac{q_{ABG}^2 r^2}{\left(q_{ABG}^2 + r^2\right)^2}, \tag{14}$$

where q_{ABG} is the electric charge and m is the ADM mass.

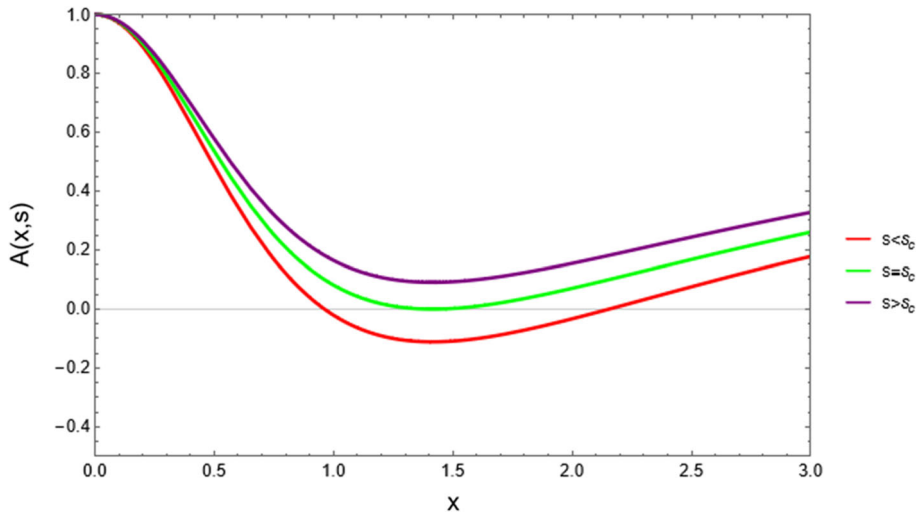

Fig. 2 Graphic representation of the auxiliary function $A(x, s)$ for Bardeen metric

The Kretschmann scalar for this metric is

$$K = 4\left(\frac{2m}{\left(q_{ABG}^2+r^2\right)^{3/2}} - \frac{q_{ABG}^2}{\left(q_{ABG}^2+r^2\right)^2}\right)^2 + \frac{16\left(m\left(-2q_{ABG}^4 - q_{ABG}^2 r^2 + r^4\right) + q_{ABG}^2(q_{ABG}-r)(q_{ABG}+r)\sqrt{q_{ABG}^2+r^2}\right)^2}{\left(q_{ABG}^2+r^2\right)^7} + \left(\frac{2q_{ABG}^2\left(q_{ABG}^4 - 8q_{ABG}^2 r^2 + 3r^4\right)}{\left(q_{ABG}^2+r^2\right)^4} - \frac{2m\left(2q_{ABG}^4 - 11q_{ABG}^2 r^2 + 2r^4\right)}{\left(q^2+r^2\right)^{7/2}}\right)^2, \tag{15}$$

which is regular in all spacetime. The function g_{tt} can also be rewritten using the substitutions $x = r/|q_{ABG}|$ and $s = |q_{ABG}|/2\,m$

$$-g_{tt} = f(r) = A(x,s) \equiv 1 - \frac{x^2}{s\left(x^2+1\right)^{3/2}} + \frac{x^2}{\left(x^2+1\right)^2}, \tag{16}$$

which has only one real value x_c and s_c, as shown in Fig. 3, these values can be found by using

$$A(x_c, s_c) = 0, \quad \frac{\partial A(x_c, s_c)}{\partial x} = 0, \tag{17}$$

and the result is $x_c \approx 1.58$ and $s_c \approx 0.317$. The interpretation of these critical values is: for $s > s_c$ there is no event horizon, for $s = s_c$ there is only one degenerated even horizon, and for $s < s_c$ there are two event horizons given by

$$r_\pm = |q_{ABG}|\left(\left(\frac{1}{4s} + \frac{\sqrt{u(s)}}{12s} \pm \frac{\sqrt{6}}{12s}\left(\frac{9}{2} - 12s^2 - \frac{u(s)}{6} - \frac{9(12s^2-1)}{\sqrt{u(s)}}\right)^{1/2}\right)^2 - 1\right)^{1/2}, \tag{18}$$

where

$$u(s) = 6\left(\frac{3}{2} - 4s^2 + s\,v(s)^{1/3} - \frac{4s\left(11s^2-3\right)}{v(s)^{1/3}}\right), \tag{19}$$

and

$$v(s) = 4\left(9s + 74s^3 + \sqrt{27(400s^6 - 112s^4 + 47s^2 - 4)}\right). \tag{20}$$

In terms of electric charge and mass we have $q_{ABG}^{ext} \approx 0.634\,m$.

In short, the black hole of Ayón-Beato and García is the first exact regular solution of the Einstein equations, as can be seen in (15). It is obtained using the non linear electrodynamics minimally coupled to general relativity, and has an electric field as its source. Further explanation of this solution can be found in [12,30,31] and the references therein.

3 Shapiro time for a general metric

The equations of motion for free particles in general relativity are the so-called geodesic equations. They are the generalization of the straight line to curved spacetime. To obtain the Shapiro time delay, we must first set up this equation for photons. The null radial geodesic equation is [36]

$$g_{\mu\nu}\dot{x}^\mu\dot{x}^\nu = 0, \tag{21}$$

for a general static and spherically symmetric spacetime we have

$$g_{tt}\dot{t}^2 + g_{rr}\dot{r}^2 + g_{\theta\theta}\dot{\theta}^2 + g_{\phi\phi}\dot{\phi}^2 = 0, \tag{22}$$

where the dot signifies a differentiation with respect to the affine parameter. Assuming that the geodesic is in the equatorial plane $\theta = \pi/2$ and the specific static and spherically symmetric configuration is given by

$$ds^2 = -B(r)dt^2 + A(r)dr^2 + C(r)\left(d\theta^2 + \sin^2\theta d\phi^2\right), \tag{23}$$

the path of a light ray is described by [58,59]

$$-B(r)\dot{t}^2 + A(r)\dot{r}^2 + C(r)\dot{\phi}^2 = 0. \tag{24}$$

This movement has two conserved quantities: the total energy, and the angular momentum. They are [60]

$$E = B(r)\dot{t}, \tag{25}$$

$$L = C(r)\dot{\phi}. \tag{26}$$

With Eqs. (24)–(26) we can write

$$\frac{d\phi}{dr} = \frac{1}{C(r)}\left[\frac{1}{A(r)B(r)}\left(\frac{1}{b^2} - \frac{B(r)}{C(r)}\right)\right]^{-1/2}, \tag{27}$$

where $b \equiv L/E$ is the impact parameter. We will explain this quantity in more detail in the next section. When the light reaches the closest approach to the black hole $r = d$, we have $dr/d\phi = 0$, i.e

$$b = \sqrt{\frac{C(d)}{B(d)}}. \tag{28}$$

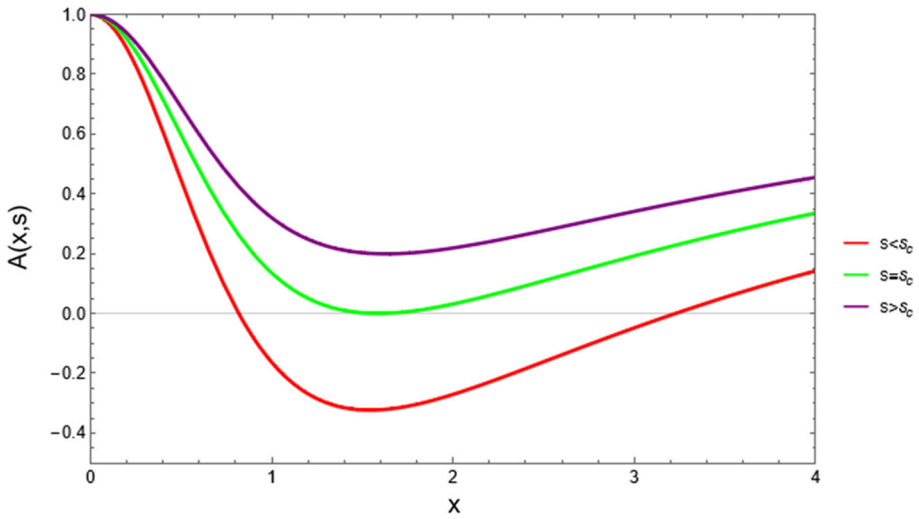

Fig. 3 Graphic representation of the auxiliary function $A(x, s)$ for Ayón-Beato and García metric

Collecting (25), (26), (27) and (28) into the geodesic equation (24) we get

$$\frac{dt}{dr} = \frac{1}{b}\sqrt{\frac{A(r)}{B(r)}}\left[\frac{1}{b^2} - \frac{B(r)}{C(r)}\right]^{-1/2}. \tag{29}$$

Then, the total time between the closest approach d and a point r_1 is

$$t(r_1, d) = \frac{1}{b}\int_d^{r_1} \sqrt{\frac{A(r)}{B(r)}}\left[\frac{1}{b^2} - \frac{B(r)}{C(r)}\right]^{-1/2} dr, \tag{30}$$

from now on we have to choose specific functions for $A(r)$, $B(r)$ and $C(r)$. Let us consider the Schwarzschild solution, which is a good approximation for the solar system. The Eq. (23) for this solution is

$$ds^2 = -\left(1 - \frac{2m}{r}\right)dt^2 + \left(1 - \frac{2m}{r}\right)^{-1} dr^2 + r^2\left(d\theta^2 + \sin^2\theta d\phi^2\right), \tag{31}$$

then (30) is

$$t(r_1, d) = \int_d^{r_1} \frac{r^2\sqrt{(d-2m)\,r}\,dr}{(r-2m)\sqrt{2d^3m - d^3r + r^3(d-2m)}}, \tag{32}$$

although the above integral can be solved analytically [61], we will use a Taylor series expansion, so that the total time

$$t(r_1, d) = \sqrt{r_1^2 - d^2} + m\left(\frac{r_1 - d}{r_1 + d}\right)^{1/2} + 2m\ln\left(\frac{r_1 + \sqrt{r_1^2 - d^2}}{d}\right) + \mathcal{O}(m^2). \tag{33}$$

Note that the first term of (33) is the result for flat spacetime. The time required for a light signal to travel from one point r_1 to another point r_2 and back for r_1 is

$$T_{SC} = 2\left(t(r_1, d) + t(r_2, d)\right) \tag{34}$$

i.e.

$$T_{SC} = 2\left(\sqrt{r_1^2 - d^2} + \sqrt{r_2^2 - d^2}\right) + 2m\left[\left(\frac{r_1 - d}{r_1 + d}\right)^{1/2} + \left(\frac{r_2 - d}{r_1 + d}\right)^{1/2}\right] + 4m\ln\left[\left(\frac{r_1 + \sqrt{r_1^2 - d^2}}{d}\right)\left(\frac{r_2 + \sqrt{r_2^2 - d^2}}{d}\right)\right]. \tag{35}$$

Assuming that $r_1 > r_2 \gg d$, the time delay (just subtract the part related to the flat case from the total) is

$$\Delta T_{SC} \simeq 4m\left[\ln\left(\frac{4r_1r_2}{d^2}\right) + 1\right], \tag{36}$$

which exactly corresponds to (1) in the international system of units. We see that the Shapiro time increases with mass and distances r_1 and r_2.

4 Impact parameter

In the previous section we used in our calculations the quantity $b \equiv L/E$, which is the effect parameter. In this section we will show how to obtain it for the general metric. First, however, it is important to clarify why you need to obtain this parameter. The same approach, i.e. $d = R_\odot$ as for the Sun, is impossible for the black hole case. One could be naive and take $d = r_+$ for this case. However, as we will show in a moment, the light (or particle) is absorbed when it is sent from a distance smaller than the critical impact parameter b_c, which is always larger than the event horizon. Since Shapiro's experiment is that the light is only slightly deflected by the

massive body, we need to know b_c for each black hole in order to choose d accordingly.

To start, we choose the equatorial plane where $\theta = \pi/2$, we have from (22)

$$g_{tt}\dot{t}^2 + g_{rr}\dot{r}^2 + g_{\phi\phi}\dot{\phi}^2 = 0, \tag{37}$$

we also have the conserved quantities, energy and momentum, respectively given by

$$g_{tt}\dot{t} = E, \tag{38}$$

$$g_{\phi\phi}\dot{\phi} = L. \tag{39}$$

Substituting these quantities into (37) we have

$$\dot{r}^2 = E^2 - V_{eff}(r), \tag{40}$$

where $V_{eff}(r) = (-g_{tt}/r^2)L^2$. Now, we will look for unstable photon orbits given by the conditions

$$\frac{dV_{eff}(r_c)}{dr} = 0, \tag{41}$$

and

$$\frac{d^2V_{eff}(r_c)}{dr^2} < 0. \tag{42}$$

In the above equations r_c is called the capture radius, this nomenclature will be justified in a moment. The first equation leads to

$$r_c g'_{tt} - 2g_{tt} = 0, \tag{43}$$

where the prime denotes a derivative with respect to the radial coordinate. And the second one is

$$r_c g''_{tt} - g'_{tt} < 0. \tag{44}$$

For Schwarzschild solution (2), for example, we have

$$V_{eff}(r) = \frac{L^2\left(1 - \frac{2m}{r}\right)}{r^2} \tag{45}$$

and by applying (41) we get $r_c = 3m$ which leads to

$$\frac{d^2V_{eff}(r_c)}{dr^2} = -\frac{2L^2}{81m^4}, \tag{46}$$

since L and m are positive quantities, (42) is satisfied. Having found the capture radius, we choose $E = V_{eff}(r_c)$ and obtain

$$\dot{\phi}(r_c) = E\left(\frac{-1}{g_{tt}g_{\phi\phi}}\right)^{1/2}, \tag{47}$$

since the definition of the impact parameter $b \equiv L/E$, we have that its value considering $r = r_c$ is

$$b_c = \frac{L(r_c)}{E(r_c)} = g_{\phi\phi}\left(\frac{-1}{g_{tt}g_{\phi\phi}}\right)^{1/2}|_{r=r_c}. \tag{48}$$

For the Schwarzschild solution $b_c = 3\sqrt{3}m$. We know that the radius of the event horizon for this solution is $r = 2m$, then the capture radius r_c and the critical impact parameter b_c are larger. In the Fig. 4 we illustrate the situation of light rays emitted from a point P_1 with different impact parameters. The black line corresponds to the event horizon of a Schwarzschild black hole. Note that for $b = b_c$, the red dotted line, the photons are trapped and begin to orbit the black hole with radius $r = r_c$ (the capture radius), in which case it is an unstable orbit. When light is sent with $b < b_c$, it is absorbed by the black hole, green line. However, if we consider $b > b_c$, blue line, the trajectory is only slightly deflected and the rays can escape the gravity of the black hole and reach the point P_2.

5 Comparison between two black holes with the same event horizon and similar masses

In this section, we begin by comparing the Shapiro time for different black hole solutions. It should be recalled that our goal is to see if it is possible to distinguish two black holes using this feature. To begin, we will compare the Schwarzschild and Reissner–Nordström solutions.

It would be interesting if we could make the event horizons and masses the same. However, if we presuppose that the horizons are equal and write the equation like this

$$2m_1 = m_2 + \sqrt{m_2^2 - q_{RN}^2}, \tag{49}$$

where m_1 and m_2 are the masses of the Schwarzschild and Reissner–Nordström black holes, respectively. Solving (49), we find that the charge q_{RN} is equal to

$$q_{RN} = 2\sqrt{m_1m_2 - m_1^2}, \tag{50}$$

this result implies that $m_1 < m_2 < 2m_1$.Therefore, the comparison is considered a proximate mass.

The situation under consideration is: what is the time delay of a light signal moving back and forth from a planet P_1 of radius r_1 to another planet P_2 of radius r_2. We assume that the planets are in superior conjunction, and $r_1 > r_2 \gg d$, where d is the distance of closest approach to the black hole located between the planets. We will always assume that d is larger than the critical impact parameter b_c of the considered solutions, so that we are dealing with a situation similar to that in the Fig. 4. We emphasize that this model is far idealized compared to the models used to measure the Shapiro effect in the solar system, but it is a good approximation to answer our motivating question. We have already calculated the total travel time (35) and the delay (36) for the Schwarzschild black hole. Before attempting to compute the integral (30) for the metric (4), we need to make a small adjustment since the Taylor series expansion gives an inconsistent result with respect to the mass. We expect the time found for the Reissner–Nordström solution to be the same as (35) at the limit $q_{RN} \to 0$, but we do not find that using

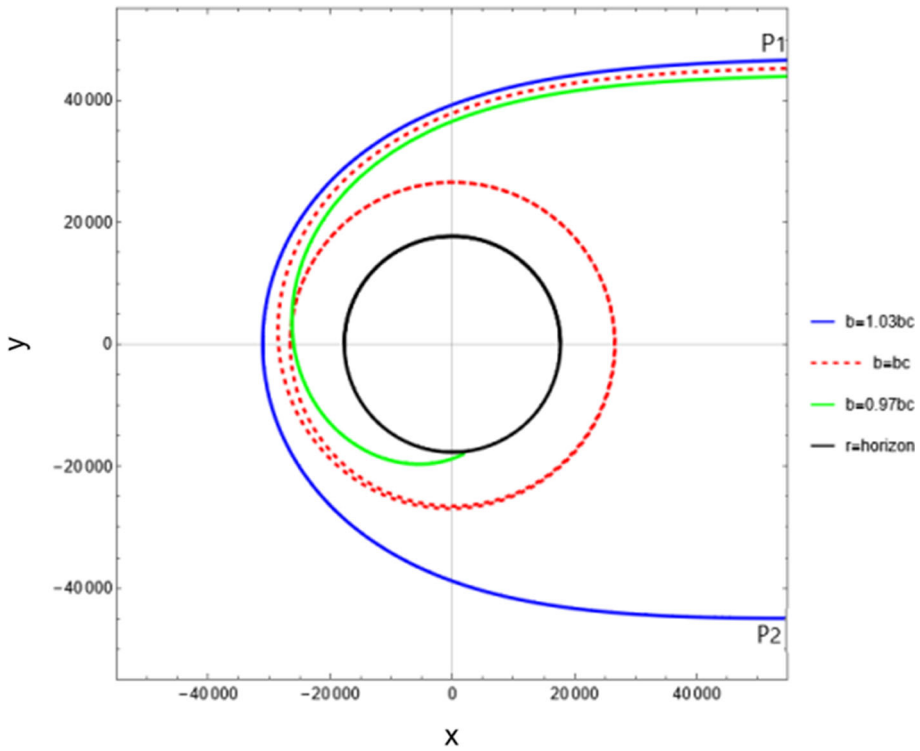

Fig. 4 Graphical representation of the light path, considering the Schwarzschild black hole, for different values of the impact parameter

the mass expansion to solve the integral (30). So we use the metric as

$$B(r) = 1 - \frac{2Gm_1}{r} + \frac{Gq_{RN}^2}{r^2},$$
$$A(r) = B(r)^{-1},$$
$$C(r) = r^2. \tag{51}$$

The justification for this insight is that, in the S.I., we have

$$-g_{tt} = 1 - \frac{2Gm_1}{c^2 r} \tag{52}$$

for the Schwarzschild, and in this case the expansion mentioned in Sect. 3 is the same whether we consider m_1 or G. If we substitute (51) into (30), we get

$$t(r_1, d) = \int_d^{r_1} \frac{r^4}{G\left(q_{RN}^2 - 2m_2 r\right) + r^2} \times \left(\frac{d^2 r^4 - \left(d^4\left(G\left(q_{RN}^2 - 2m_2 r\right) + r^2\right)\right) - 2dGm_2 r^4 + Gq_{RN}^2 r^4}{d^2 - 2dGm_2 + Gq_{RN}^2}\right)^{-1/2} dr, \tag{53}$$

and after a Taylor series expansion we can integrate the above equation and get

$$t(r_1, d) = \sqrt{r_1^2 - d^2} - \frac{3Gq_{RN}^2 \cot^{-1}\left(\frac{d}{\sqrt{r_1^2 - d^2}}\right)}{2d} + Gm_2\left(\frac{r_1 - d}{r_1 + d}\right)^{1/2} + 4Gm_2 \tanh^{-1} \times \left(\sqrt{\frac{r_1 - d}{r_1 + d}}\right) + \mathcal{O}(G^2). \tag{54}$$

Note that if we put $q_{RN} = 0$ and $G = 1$ in (54) the result will be exactly (33) [62]. Note that

$$tanh^{-1}(u) = \frac{1}{2} ln\left(\frac{1+u}{1-u}\right). \tag{55}$$

The total travel time is

$$T_{RN} = 2\left(t(r_1, d) + t(r_2, d)\right) = 2\left(\sqrt{r_1^2 - d^2} + \sqrt{r_2^2 - d^2}\right) - \frac{3Gq_{RN}^2\left[\cot^{-1}\left(\frac{d}{\sqrt{r_1^2 - d^2}}\right) + \cot^{-1}\left(\frac{d}{\sqrt{r_2^2 - d^2}}\right)\right]}{d} + 2Gm_2\left[\left(\frac{r_1 - d}{r_1 + d}\right)^{1/2} + \left(\frac{r_2 - d}{r_2 + d}\right)^{1/2}\right] + 8Gm_2\left[\tanh^{-1}\left(\sqrt{\frac{r_1 - d}{r_1 + d}}\right) + \tanh^{-1}\left(\sqrt{\frac{r_2 - d}{r_2 + d}}\right)\right], \tag{56}$$

and the Shapiro time delay, with $r_1 \gg d$ and $r_2 \gg d$ is,

$$\Delta T_{RN} = 4Gm_2\left[\ln\left(\frac{4r_1 r_2}{d^2}\right) + 1\right] + 3Gq_{RN}^2\left(\frac{1}{r_1} + \frac{1}{r_2} - \frac{\pi}{d}\right). \tag{57}$$

The part of the charge in the above equation has a negative sign, so it reduces the difference between the total relativis-

tic time and the time for the plane case. If we consider the expressions (54), (57), and the expressions referring to the Schwarzschild solution (35) and (36), we might try to conclude that it is indeed possible to distinguish them by experiments with round-trip light signals. But this would be a hasty conclusion, because such measurements have a certain accuracy limit, which does not always meet the requirements of the theoretical model.

The last step before the numerical comparison is to calculate the critical impact parameter for the Reissner–Nordström solution. Following the procedure described in Sect. 4, one finds

$$b_c^{RN} = \frac{1}{2}\left(\sqrt{9m_2^2 - 8q_{RN}^2} + 3m_2\right)^2 \sqrt{\frac{1}{2m_2\left(\sqrt{9m_2^2 - 8q_{RN}^2} + 3m_2\right) - 4q_{RN}^2}}. \tag{58}$$

Let us now compare the Shapiro time delay for these two solutions. Since we are going to make a numerical comparison, we choose the values of some constants. We have chosen the masses as

$$\begin{aligned} m_1 &= 6.0 \times M'_\odot, \\ m_2 &= 6.1 \times M'_\odot, \end{aligned} \tag{59}$$

where $M'_\odot$ is the solar mass in the geometrized units

$$\begin{aligned} M'_\odot &= \frac{M_\odot}{c^2 G^{-1}} \\ &= \frac{1.98892 \times 10^{30}\text{kg}}{\left(2.99 \times 10^8 \text{m/s}\right)^2 \left(6.67408 \times 10^{-11}\text{Nm}^2/\text{kg}^2\right)^{-1}} \\ &= 1484.06\text{m}. \end{aligned} \tag{60}$$

We affirm that geometrized units are powers of length (m). The masses in (59) are characteristic of so-called stellar black holes, they lead, when put into (50), to the charge $q_{RN} = 2299.1$. That is, these choices lead to the following event horizons

$$\begin{aligned} 2m_1 &= 17808.8, \\ m_2 + \sqrt{m_2^2 - q_{RN}^2} &= 17808.8. \end{aligned} \tag{61}$$

Furthermore, the critical impact parameters for both solutions are

$$\begin{aligned} b_c^{SC} &= 46268.6, \\ b_c^{RN} &= 46527.5. \end{aligned} \tag{62}$$

Given these values, we choose $d = 46600$. This value is nothing special compared to all others larger than 46527.5, the value of the largest critical impact parameter considered. The distances between the planets and d will be

$$r_1 = 2.0 \times 10^4 d,$$

$$r_2 = 1.0 \times 10^4 d. \tag{63}$$

In this case we stick to the relations $r_1 > r_2 \gg d$. These distances are on the order of 10^8 m, so the travel time between them is on the order of seconds. Note that, again, there is nothing special about these specific selections. Moreover, there is no realistic scenario associated with these choices, we just have to choose values that are associated with (36) and (57). Then we have

$$\Delta T_{SC} = 765782, \tag{64}$$

and

$$\Delta T_{RN} = 778010. \tag{65}$$

We can already see that there is a difference in the result of the solutions, but the interpretation based on the geometrized units is not our subject. To convert time to the international system of units (S.I.), simply divide the value in geometric units by c (speed of light in vacuum). So in S.I. we have

$$\Delta T'_{SC} = \frac{\Delta T_{SC}}{c} = 2.55261 \times 10^{-3}\ \text{s}, \tag{66}$$

and

$$\Delta T'_{RN} = \frac{\Delta T_{RN}}{c} = 2.59337 \times 10^{-3}\ \text{s}. \tag{67}$$

Note that the difference in the Shapiro time delay for these solutions is on the order of 10^{-5} s. Our optical clocks on the ground have sufficient precision to measure this time [63–65]. So in this idealized situation, the solutions are distinguishable by the Shapiro delay time. But in a realistic situation, of course, this experiment would require a more precise model, and this time scale might be difficult to achieve. Instead of choosing arbitrary distances and masses, you can use the values from the Earth–Sun–Venus case. Note, however, that this would not lead to a better or even more realistic result than the one presented above. There would also be a difference found between the delay times, only they would be smaller than those we found here. There is a way to make the difference between the times larger than those found in the previous example. If we look at the expressions (36) and (57), we find that the delay is proportional to the mass. So let us check how the Shapiro time is for a supermassive black hole. For this purpose, we will now choose

$$\begin{aligned} m_1 &= 3.4 \times 10^9 \times M'_\odot, \\ m_2 &= 3.6 \times 10^9 \times M'_\odot, \end{aligned} \tag{68}$$

then we have $q_{RN} = 2.44758 \times 10^{12}$, and

$$\begin{aligned} b_c^{SC} &= 2.62189 \times 10^{13}, \\ b_c^{RN} &= 2.67467 \times 10^{13}. \end{aligned} \tag{69}$$

Considering these values, we choose $d = 2.7 \times 10^{13}$ (again, we have free choice for this distance as long as the no-return condition is observed $d > b_c$), $r_1 = 2.0 \times 10^2 d$, and $r_2 =$

$1.0 \times 10^2 d$. In this example, the closest approach is on the order of 10^{13} m, i.e., two orders of magnitude greater than the distances in the Earth–Sun–Venus experiment. For this reason, we have chosen r_1 and r_2 such that the distances can be traveled with light on a time scale of years (10^{15} m leads to a time travel of about 1.05 years). Of course, since these parameters are the same for both types of black holes, our object of study does not depend on this choice. However, we know that in a real observational situation we are limited to the human time scale. Moreover, we know that observations made from very distant regions (outside the solar system) have more complications and experimental errors than those made at shorter distances. Thus we have that the time delays are

$$\Delta T'_{SC} = 826827 \text{ s} \approx 9.6 \text{ days}, \tag{70}$$

and

$$\Delta T'_{RN} = 872012 \text{ s} \approx 10.1 \text{ days}. \tag{71}$$

An important detail is that in the two cases considered, the delay of the Reissner–Nordström black hole was larger. This was to be expected since we consider $m_2 > q_{RN}$ for both examples and this implies that the mass term dominates the Eq. (57). As we can see, the difference in time delay is now on the order of hours. In Figs. 5 and 6 we show the time delay for a set of values of r_1, r_2 with fixed masses, charge, and d. It is interesting to realize that in this case the mass term in the expression (57) prevails, therefore the Reissner–Nordström solution present a larger delay than the Schwarzschild. In Figs. 7 and 8 we vary the mass and the distance r_1. As we expected when considering the analytic expressions, the Shapiro time increases when we increase the mass or the distances r_1 and r_2. These four figures also show that we are free to choose the parameters. The values are slightly different, but the behavior of the Shapiro time is practically the same for both solutions. This is also true for the regular solutions, which we will discuss in the next section. Therefore, we will not make these diagrams for them, as this would be a repetition.

6 Comparison between three black holes with the same event horizon and masses

In this section we will compare the Shapiro time for the solutions of Reissner–Nordström, Bardeen and Ayón-Beato and García (ABG). For the first one, we already have the necessary expressions. For the Bardeen metric, the Eq. (30) becomes

$$t(r_1, d) = \int_d^{r_1} \left(\frac{\frac{1}{d^2} - \frac{2m_3}{\left(d^2+q_{BD}^2\right)^{3/2}}}{2m_3\left(\frac{1}{\left(q_{BD}^2+r^2\right)^{3/2}} - \frac{1}{\left(d^2+q_{BD}^2\right)^{3/2}}\right) + \frac{1}{d^2} - \frac{1}{r^2}} \right)^{1/2} \left(1 - \frac{2m_3 r^2}{\left(q_{BD}^2+r^2\right)^{3/2}}\right)^{-1} dr, \tag{72}$$

where m_3 is the mass and q_{BD} is the magnetic charge. Again, we use a Taylor series expansion to solve the integral, which leads to the following result

$$\begin{aligned} t(r_1, d) = {} & \sqrt{r_1^2 - d^2} - \frac{m_3 q_{BD}^2 \left(3d^2 + 2q_{BD}^2\right)\sqrt{r_1^2 - d^2}}{\left(d^2 + q_{BD}^2\right)^2 \sqrt{r_1^2 + q_{BD}^2}} \\ & + 2m_3 \ln\left(\sqrt{r_1^2 - d^2} + \sqrt{r_1^2 + q_{BD}^2}\right) - 2m_3 \ln\left(d^2 + q_{BD}^2\right) \\ & + \frac{d^4 m_3 \sqrt{r_1^2 + q_{BD}^2}}{\sqrt{r_1^2 - d^2}\left(d^2 + q_{BD}^2\right)^2} \\ & - \frac{d^4 m_3}{\sqrt{r_1^2 - d^2}\left(d^2 + q_{BD}^2\right)^{3/2}} + \mathcal{O}(m^2). \end{aligned} \tag{73}$$

This is the time required for light to travel from the point of closest approach d to the general point r_1. Consider the same situation as in the previous section, i.e., the light is sent from one planet at r_1 to another at r_2, these bodies being at superior conjunction, and reflected back to r_1; the total time is $2\left(t(r_1, d) + t(r_2, d)\right)$. Then we have

$$\begin{aligned} T_{BD} = {} & 2\left(\sqrt{r_1^2 - d^2} + \sqrt{r_2^2 - d^2}\right) \\ & - \frac{2m_3 q_{BD}^2 \left(3d^2 + 2q_{BD}^2\right)}{\left(d^2 + q_{BD}^2\right)^2}\left(\frac{\sqrt{r_1^2 - d^2}}{\sqrt{r_1^2 + q_{BD}^2}} + \frac{\sqrt{r_2^2 - d^2}}{\sqrt{r_2^2 + q_{BD}^2}}\right) \\ & - 4m_3 \ln\left(d^2 + q_{BD}^2\right) \\ & + 4m_3 \ln\left[\left(\sqrt{r_1^2 - d^2} + \sqrt{r_1^2 + q_{BD}^2}\right)\left(\sqrt{r_2^2 - d^2} + \sqrt{r_2^2 + q_{BD}^2}\right)\right] \\ & + \frac{2d^4 m_3}{\left(d^2 + q_{BD}^2\right)^2}\left(\frac{\sqrt{r_1^2 + q_{BD}^2}}{\sqrt{r_1^2 - d^2}} + \frac{\sqrt{r_2^2 + q_{BD}^2}}{\sqrt{r_2^2 - d^2}}\right) \\ & - \frac{2d^4 m_3}{\left(d^2 + q_{BD}^2\right)^{3/2}}\left(\frac{1}{\sqrt{r_1^2 - d^2}} + \frac{1}{\sqrt{r_2^2 - d^2}}\right). \end{aligned} \tag{74}$$

The effect we are concerned with here is only the relativistic travel time delay in comparison to the flat case, which is

$$\begin{aligned} \Delta T_{BD} = 2\Bigg[& - 2m_3 \ln\left(d^2 + q_{BD}^2\right) \\ & - 2m_3\left(\frac{1}{\sqrt{\frac{q_{BD}^2}{r_1^2} + 1}} + \frac{1}{\sqrt{\frac{q_{BD}^2}{r_2^2} + 1}}\right) \end{aligned}$$

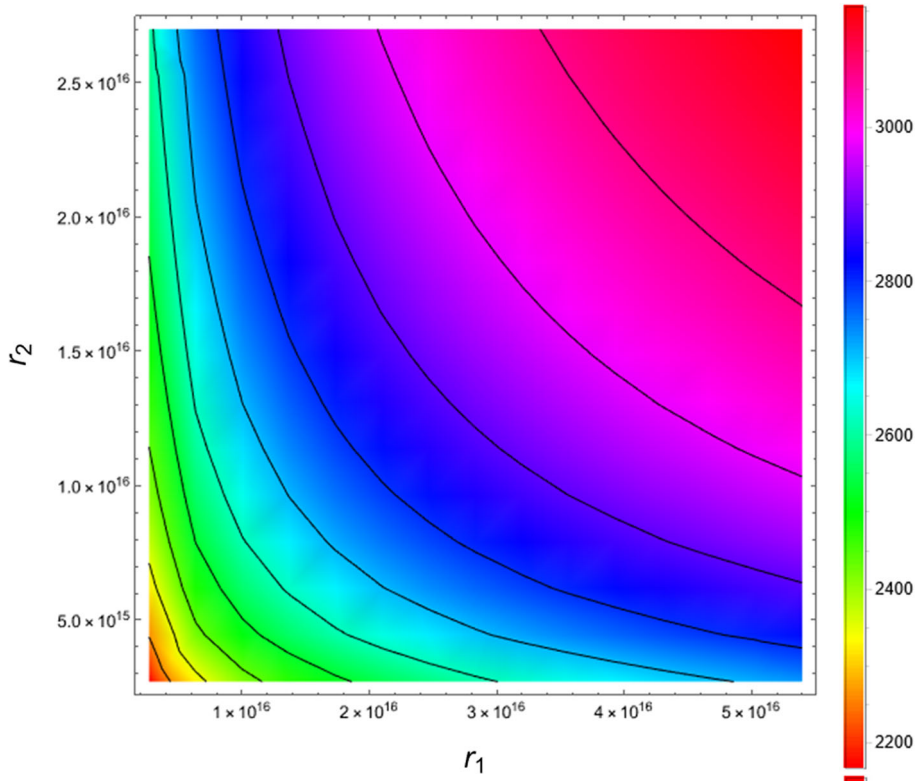

Fig. 5 Graphical representation of the delay time (in hours) of the Schwarzschild solution, with $m_1 = 3.4 \times 10^9 \times M'_{\odot}$ and $d = 2.7 \times 10^{13}$. We adjust $100d < r_1 < 2 \times 10^3 d$ and $100d < r_2 < 1 \times 10^3 d$

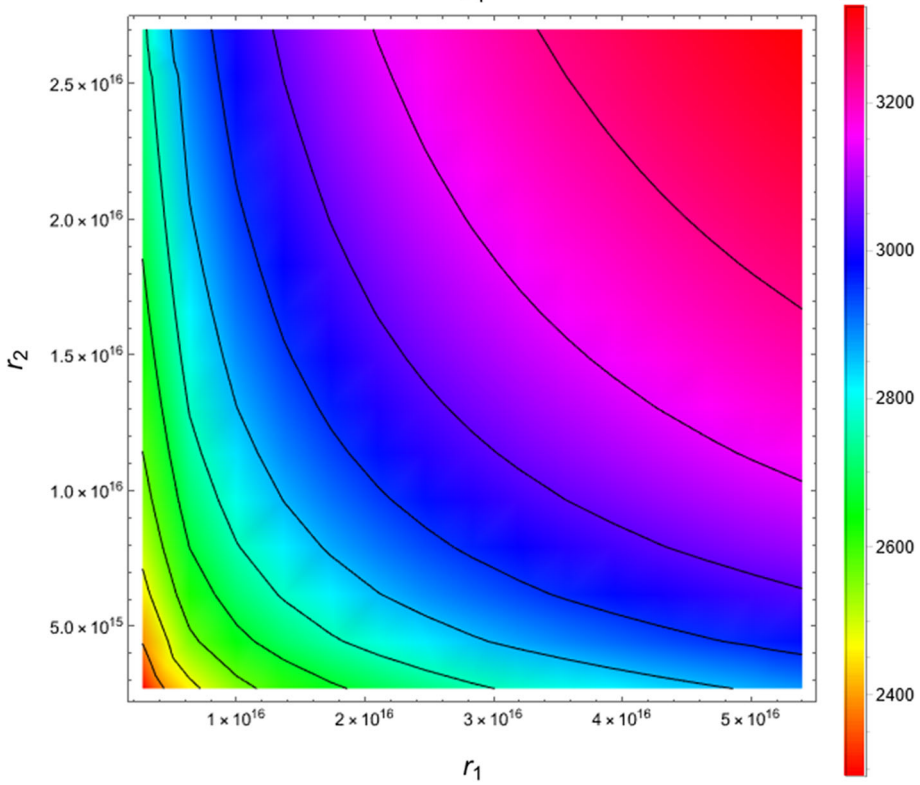

Fig. 6 Graphical representation of the delay time (in hours) of the Reissner–Nordström solution, with $m_2 = 3.6 \times 10^9 \times M'_{\odot}$, $q_{RN} = 2.44758 \times 10^{12}$ and $d = 2.7 \times 10^{13}$. We adjust $100d < r_1 < 2 \times 10^3 d$ and $100d < r_2 < 1 \times 10^3 d$

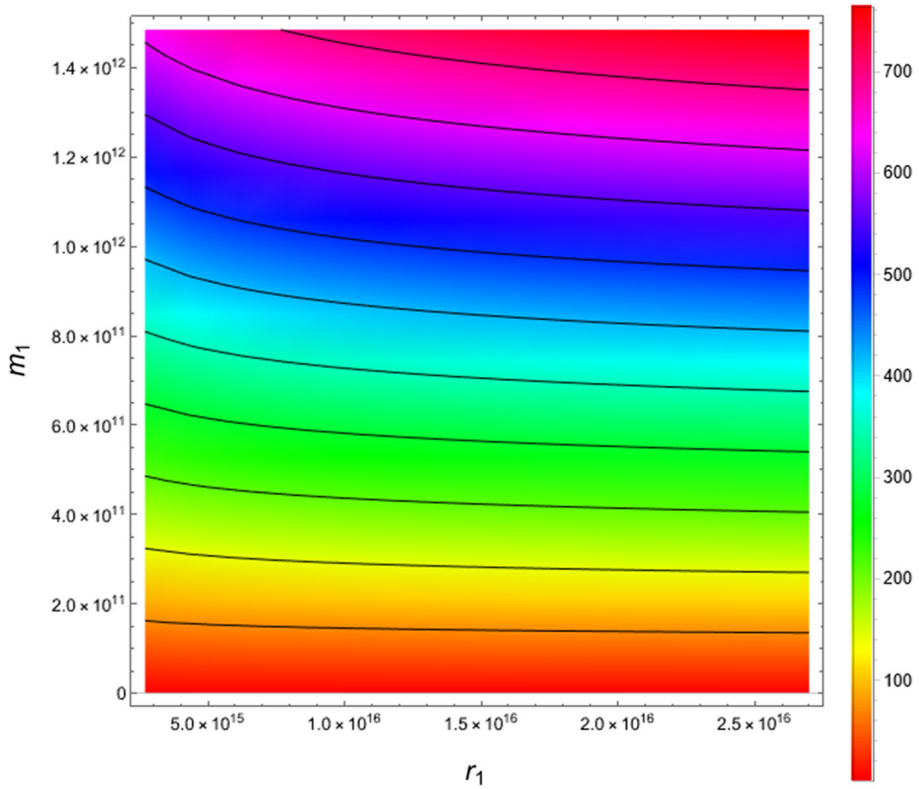

Fig. 7 Graphical representation of the delay time (in hours) of the Schwarzschild solution, with $d = 2.7 \times 10^{13}$, and $r_2 = 10^2 d$. The mass m_1 is varying in an interval from $m_1 = 10^6 \times M_\odot$ to $m_1 = 10^9 \times M_\odot$

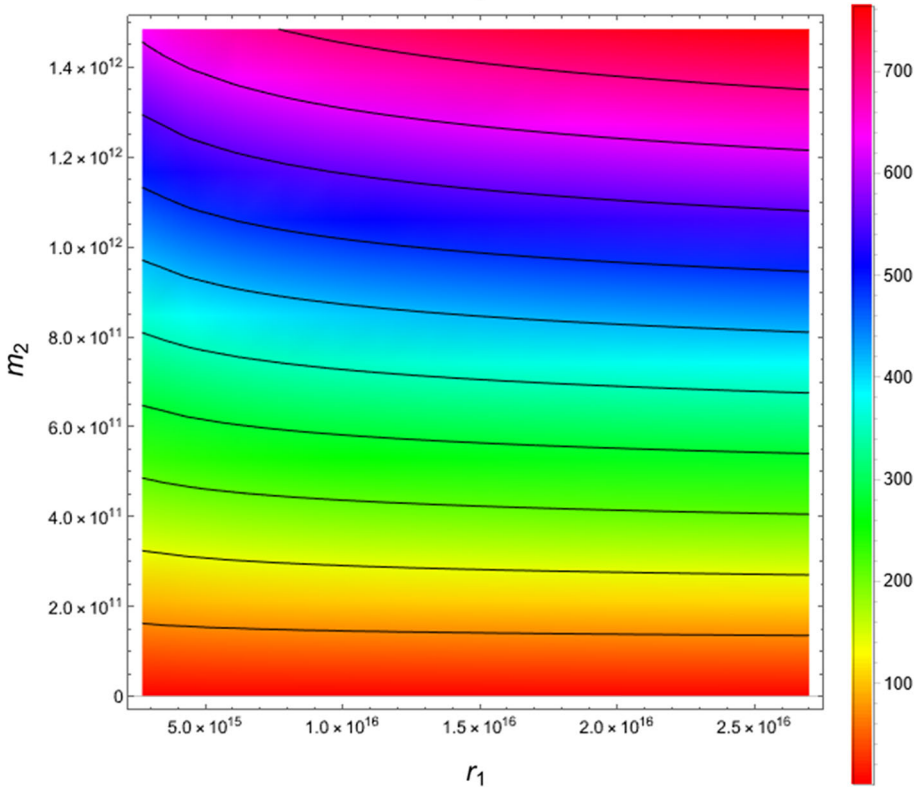

Fig. 8 Graphical representation of the delay time (in hours) of the Reissner–Nordström solution, with $d = 2.7 \times 10^{13}$, $q_{RN} = 1.9 \times 10^{11}$, and $r_2 = 10^2 d$. The mass m_2 is varying in an interval from $m_2 = 10^6 \times M_\odot$ to $m_2 = 10^9 \times M_\odot$

$$+2m_3 \ln\left(\left(r_1\sqrt{\frac{q_{BD}^2}{r_1^2}+1}+r_1\right)\times\left(r_2\sqrt{\frac{q_{BD}^2}{r_2^2}+1}+r_2\right)\right)\Bigg], \tag{75}$$

where we use the approximation $r_1 \gg d$ and $r_2 \gg d$. It is worth noting that, as expected, both (73) and (75) give the same results as in the Schwarzschild case when the magnetic charge is zero.

For the ABG solution (14) we have the same integrand as (53), this is of course the same consideration as using the Taylor series expansion for the gravitational constant G instead of the black hole mass. So the result is

$$t(r_1,d) = \sqrt{r_1^2-d^2} - \frac{3Gq_{ABG}^2\cot^{-1}\left(\frac{d}{\sqrt{r_1^2-d^2}}\right)}{2d} + Gm_4\left(\frac{r_1-d}{r_1+d}\right)^{1/2} + 4Gm_4\tanh^{-1}\left(\sqrt{\frac{r_1-d}{r_1+d}}\right) + \mathcal{O}(G^2), \tag{76}$$

where m_4 is the mass and q_{ABG} is the electric charge. Considering the same situation as above, the total time is

$$T_{ABG} = 2\left(\sqrt{r_1^2-d^2}+\sqrt{r_2^2-d^2}\right) - \frac{3Gq_{ABG}^2\left[\cot^{-1}\left(\frac{d}{\sqrt{r_1^2-d^2}}\right)+\cot^{-1}\left(\frac{d}{\sqrt{r_2^2-d^2}}\right)\right]}{d} + 2Gm_4\left[\left(\frac{r_1-d}{r_1+d}\right)^{1/2}+\left(\frac{r_2-d}{r_2+d}\right)^{1/2}\right] + 8Gm_4\left[\tanh^{-1}\left(\sqrt{\frac{r_1-d}{r_1+d}}\right)+\tanh^{-1}\left(\sqrt{\frac{r_2-d}{r_2+d}}\right)\right], \tag{77}$$

and the Shapiro time delay, with $r_1 \gg d$ and $r_2 \gg d$, is

$$\Delta T_{ABG} = 4Gm_4\left[\ln\left(\frac{4r_1r_2}{d^2}\right)+1\right] + 3Gq_{ABG}^2\left(\frac{1}{r_1}+\frac{1}{r_2}-\frac{\pi}{d}\right). \tag{78}$$

Note that the Shapiro time for Reissner–Nordström and ABG would be the same only if we consider a situation where $m_2 = m_4$ and $q_{RN} = q_{ABG}$. Since we choose to align the masses and event horizons, we will have different charges, and thus the times will be different.

To begin with, we will choose the masses as

$$m_2 = m_3 = m_4 = 6.1 \times M'_\odot, \tag{79}$$

and the event horizon for all three solutions

$$r_+ = 17808.8. \tag{80}$$

These choices immediately lead to

$$q_{RN} = 2299.1. \tag{81}$$

We can calculate numerically the other charges q_{BD} and q_{ABG}

$$q_{BD} = 1874.62, \quad q_{ABG} = 1454.32. \tag{82}$$

The critical impact parameters are

$$b_c^{RN} = 46527.5,\quad b_c^{BD} = 42464.2,\quad b_c^{ABG} = 42538.7. \tag{83}$$

From the same intuition as in the previous section, we choose $d = 46600$ since it is larger than these three values. The radii of the planets will be

$$r_1 = 2.0\times10^4 d,\quad r_2 = 1.0\times10^4 d. \tag{84}$$

We have compiled the results obtained by these decisions in the Table 1. Recall that in the examples we chose the same event horizon for the 4 solutions and the same distances r_1, r_2, and d. Also note that when the unit is not specified, we consider geometrized units. Namely, mass, charge, and time have the unit of length (m). As we can see, for stellar black hole magnitudes, there is no difference in the results down to the order of milliseconds. The shortest delay was for the Bardeen solution and the longest for the Reissner–Nordström. This is interesting because it shows that even when the critical charge condition is met, $q_{BD} < 4/3\sqrt{3}m_3$,and has a slightly larger mass; in the Bardeen solution, the delay is smaller than in Schwarzschild. This is due to the negative components in the expression (75), which are always associated with the magnetic charge. The results we obtained for the Reissner–Nordström and ABG solutions were most similar, which was to be expected since their analytical expressions (54) and (76) are identical. To justify once again our freedom in the choice of parameters, we show in Table 2 (the masses and charges are the same as in this example) the Shapiro time of these 3 solutions for a range of d, r_1 and r_2. In this table $r_1 = 120d, 240d, 350d$ and $r_2 = 100d, 200d, 300d$ for each d value. We can also see that the Shapiro time is proportional to these parameters.

If we now consider supermassive black holes, with the masses

$$m_2 = m_3 = m_4 = 3.6\times10^9 \times M'_\odot, \tag{85}$$

and event horizon

$$r_+ = 1.00916\times10^{13}. \tag{86}$$

Furthermore, we use the same values for the distances as in the last section, i.e.

$$d = 2.7 \times 10^{13},$$
$$r_1 = 2.0 \times 10^2 d,$$
$$r_2 = 1.0 \times 10^2 d. \tag{87}$$

We have the following results shown in the Table 3. The event horizon for the 4 solutions and the distances r_1, r_2 and d are identical. The Bardeen solution had the shortest delay, and the ABG solution had the longest. The difference between these results is about 58.7 h. All of the delays were on the order of days. This is because the expressions are proportional to mass and we are working with masses billions of times larger than the mass of the Sun. The density plots Figs. 5, 6, 7 and 8 show the dependence of the Shapiro time on the distances r_1 and r_2, and on the masses. As we can see, there is nothing special about the choice of these parameters, they are simply values that satisfy the conditions imposed. Any other choice, whether it comes from a real situation or not, leads to the same results that we find in our particular example. The same is true for stellar black holes, as we can see in Table 2. To return to our motivating question: Is it possible to distinguish between different black hole solutions using the Shapiro time delay? We conclude that the solutions are analytically distinguishable, except for Reissner–Nordström and Ayón-Beato and García, which are identical. Moreover, they are distinguishable even considering an idealized numerical model.

7 Conclusion

In this work, the Shapiro time delay is calculated for four solutions to investigate whether it is possible to distinguish between them. The motivation came from the idea, which appears in some papers, that regular solutions are indistinguishable from standard solutions [30,31]. Of course, there are also mentions to the contrary [33,34]; the results here point in that direction. The solutions used were Schwarzschild (mass only), Reissner–Nordström (RN) (mass and electric charge), Bardeen (mass and magnetic charge), and Ayón-Beato and García (ABG) (mass and electric charge). The Schwarzschild and RN black holes are singular, while the Bardeen and ABG black holes are regular. We point out here some of the main features of these solutions. We also show how to obtain the Shapiro time for any metric. This topic is widely used in the literature and is even covered in some textbooks, since it is one of the tests of general relativity. However, as far as we know, this is the first time that the Shapiro time has been calculated for Bardeen and ABG solutions.

We started in Sect. 2 to show the metric and some properties of the black hole solutions we will use. In Sect. 3 we assume an idealized situation similar to the one used in experiments to test general relativity [37]. Therefore, we are trying to calculate the time it takes for a light signal to travel from one planet to another when they are in a configuration called a Superior Conjunction, i.e., when they form a straight line passing through a more massive body in between (the Sun, a star, or a black hole). The calculated time is longer than if the massive body were not present, i.e., there is a delay in relativistic time relative to time for flat space. In other words: We show how to calculate the Shapiro time delay for a general static and spherically symmetric metric. The result depends on the parameters of the solution; in the Schwarzschild case, we have only the mass, the distance of closest approach to the central body d, and the distances from d to the planets, denoted r_1 and r_2.

To compare the observational result with his theoretical prediction, Shapiro used $d = R_\odot$ [36], in the case of black holes $d = r_+$ would then be most intuitive. However, as we showed in Sect. 4, photons are captured by these bodies at distances less than or equal to the critical impact parameter, which is usually larger than the event horizon. We calculate the critical impact parameters for general static and spherically symmetric metrics, and in our further numerical examples we choose d to be larger than b_c of the solutions in question.

In Sect. 5 we compare the Shapiro time of Schwarzschild and RN solutions. The analytical results for the time delay were obtained by considering first order expansions of the mass, Schwarzschild, and the gravitational constant G, RN. The expression for the RN solution returns the Schwarzschild expression when the charge is zero, and we found that the result is symmetric at charge $q \to -q$ and that it acts to decrease the delay. There could be a configuration of charge and mass where the relativistic time is smaller than the flat time, but we ruled out this possibility of a lead by always considering charges smaller than the critical one. We performed two types of numerical examples, one for masses on the order of the solar mass, stellar black holes, and another for masses billions of times larger than the solar mass, supermassive black holes. We chose the values for the masses considering the condition (50) and then found the value of the charge of the RN solution, which assumes that both bodies have the same event horizon. With the value chosen for the masses, we calculate the critical impact parameter for both solutions and choose d, r_1 and r_2. We find a difference in the delay time of the order of $10^{-5}s$ for the first example. Since the expressions (36) and (57) are proportional to mass, we find a difference in delay time on the order of hours for the second example.

In Sect. 6 we compare RN, Bardeen and ABG solutions. Analytical results for the Shapiro time delay were obtained

Table 1 Stellar black holes

Solution	Mass $(M'_{\odot})$	Charge (m)	Total time (s)	Delay time (ms)
Schwarzschild	6.0	0	9.32	2.55261
Reissner–Nordström	6.1	2299.1	9.32	2.59337
Bardeen	6.1	1874.62	9.32	2.23284
ABG	6.1	1454.32	9.32	2.59159

Table 2 Dependence of the Shapiro time delay (in seconds) on distances

d	r_1	r_2	$\Delta T'_{RN}$	$\Delta T'_{BD}$	$\Delta T'_{ABG}$
46600	5592000	4660000	0.00141822	0.00105946	0.00142035
46600	11184000	9320000	0.00158554	0.00122679	0.00158768
46600	16310000	13980000	0.00168002	0.00132127	0.00168216
60000	7200000	6000000	0.00141901	0.00105954	0.00142067
60000	14400000	12000000	0.00158634	0.00122687	0.00158799
60000	21000000	18000000	0.00168082	0.00132135	0.00168247
74000	8880000	7400000	0.00141954	0.00105958	0.00142087
74000	17760000	14800000	0.00158686	0.00122691	0.0015882
74000	25900000	22200000	0.00168134	0.00132139	0.00168268
90000	10800000	9000000	0.00141993	0.0010596	0.00142103
90000	21600000	18000000	0.00158726	0.00122693	0.00158836
90000	31500000	27000000	0.00168174	0.00132142	0.00168284

Table 3 Supermassive black holes

Solution	Mass $(10^9 \times M'_{\odot})$	Charge (m)	Total time (s)	Delay time (s)
Schwarzschild	3.4	0	5.4825×10^7	826827
Reissner–Nordström	3.6	2.44758×10^{12}	5.48666×10^7	868527
Bardeen	3.6	1.98887×10^{12}	5.48713×10^7	661373
ABG	3.6	1.54885×10^{12}	5.48708×10^7	872686

by considering first order expansions for the mass, Bardeen, and gravitational constant G, RN and ABG. The expressions for all charged solutions yield the Schwarzschild expression when the charge is zero. Moreover, they have a symmetry at charge $q \to -q$, and this acts to reduce the retardation. This is an effect opposite to that of mass. For the numerical analysis we proceed similarly to the previous section, except that now the masses of the black holes are equal. With this, we have calculated the charges and chosen the same value for the event horizon that we found earlier. The solutions of RN and ABG, which have the same expressions for the travel time, had different electric charges. Nevertheless, the times found for these solutions were closest. For example, the time delay considering the stellar black hole can only be shifted on the order of microseconds (10^{-6} s). Bardeen's solution produced the smallest time delay in the two cases considered. This shows that the magnetic charge has an opposite effect to the mass, i.e., it decreases the travel time. In fact, this is also true for the electric charges in (57) and (78), but the numerical values we chose and the critical charge limit caused the mass term to dominate these expressions. We compiled all the information in Tables 1 and 3. Although we used an idealized numerical model, we believe that the Shapiro time can be used to distinguish between different types of black holes.

In a future work, we hope to improve our results by using larger orders of approximation and adding the correction for velocity terms v/c [41]. This could, for example, lead to an analytical difference in the results of Reissner–Nordström and Ayón-Beato and García. Another perspective is to consider what effect rotation has on the Shapiro time delay. There are already some regular solutions involving rotation [66–68]; and a recent work [32] has shown by shadow analysis that Bardeen-type, Hayward-type [69], and Culetu-type [70] solutions with rotation are indistinguishable from the Kerr solution.

Acknowledgements M. E. R. thanks Conselho Nacional de Desenvolvimento Científico e Tecnológico-CNPq, Brazil, for partial financial support. This study was financed in part by the Coordenação de Aperfeiçoamento de Pessoal de Nível Superior-Brasil (CAPES)-Finance Code 001.

Data Availability Statement This manuscript has no associated data or the data will not be deposited. [Authors' comment: The authors confirm that there is no data related to the article, due to the research being theoretical.]

Funded by SCOAP[3]. SCOAP[3] supports the goals of the International Year of Basic Sciences for Sustainable Development.

References

1. K. Schwarzschild, On the gravitational field of a mass point according to Einstein's theory. Sitzungsber. Preuss. Akad. Wiss. Berlin (Math. Phys.), pp. 189–196 (1916). arXiv:physics/9905030
2. J. Stachel, R. Penrose, *Einstein's Miraculous Year: Five Papers That Changed the Face of Physics* (Princeton University Press, Princeton, 2005)
3. R. Wald, *General Relativity* (The University of Chicago Press, London, 1984)
4. H. Stephani, D. Kramer, M. MacCallum, C. Hoenselaers, E. Herlt, *Exact Solutions of Einstein's Field Equations*, 2nd edn. Cambridge Monographs on Mathematical Physics. (Cambridge University Press, Cambridge, 2003). https://doi.org/10.1017/CBO9780511535185
5. K. Akiyama et al. (Event Horizon Telescope), First M87 Event Horizon Telescope results. I. The shadow of the supermassive black hole. Astrophys. J. **875**(1), L1 (2019). arXiv:1906.11238 [astro-ph.GA]
6. K. Akiyama et al. (Event Horizon Telescope), First M87 Event Horizon Telescope results. II. Array and instrumentation. Astrophys. J. Lett. **875**(1), L2 (2019). arXiv:1906.11239 [astro-ph.IM]
7. K. Akiyama et al. (Event Horizon Telescope), First M87 Event Horizon Telescope results. III. Data processing and calibration. Astrophys. J. Lett. **875**(1), L3 (2019). arXiv:1906.11240 [astro-ph.GA]
8. K. Akiyama et al. (Event Horizon Telescope), First M87 Event Horizon Telescope results. IV. imaging the central supermassive black hole. Astrophys. J. Lett. **875**(1), L4 (2019). arXiv:1906.11241 [astro-ph.GA]
9. K. Akiyama et al. (Event Horizon Telescope), First M87 Event Horizon Telescope results. V. Physical origin of the asymmetric ring. Astrophys. J. Lett. **875**(1), L5 (2019). arXiv:1906.11242 [astro-ph.GA]
10. K. Akiyama et al. (Event Horizon Telescope), First M87 Event Horizon Telescope results. VI. The shadow and mass of the central black hole. Astrophys. J. Lett. **875**(1), L5 (2019). arXiv:1906.11243 [astro-ph.GA]
11. J.M. Bardeen, Non-singular general relativistic gravitational collapse, in *Proceedings of International Conference GR5, Tbilisi, U.S.S.R.* (1968)
12. E. Ayon-Beato, A. Garcia, Regular black hole in general relativity coupled to nonlinear electrodynamics. Phys. Rev. Lett. **80**, 5056–5059 (1998). https://doi.org/10.1103/PhysRevLett.80.5056. arXiv:gr-qc/9911046
13. M. Born, L. Infeld, Foundations of the new field theory, in *Proceedings of the Royal Society A: Mathematical, Physical and Engineering Sciences*, vol. 144, no. 852 (The Royal Society, 1934), pp. 425–451. Disponível em: https://doi.org/10.1098/rspa.1934.0059
14. E. Ayon-Beato, A. Garcia, The Bardeen model as a nonlinear magnetic monopole. Phys. Rev. Lett. B **493**, 149–152 (2000). https://doi.org/10.1016/S0370-2693(00)01125-4
15. M.E. Rodrigues, E.L.B. Junior, M.V. de S. Silva, Using dominant and weak energy conditions for building new classes of regular black holes. JCAP **02**, 059 (2018). arXiv:1705.05744 [physics.gen-ph]
16. I. Dymnikova, Regular electrically charged structures in nonlinear electrodynamics coupled to general relativity. Class. Quantum Gravity **21**, 4417 (2004). arXiv:gr-qc/0407072
17. M.E. Rodrigues, M.V. de S. Silva, Bardeen regular black hole with an electric source. JCAP **06**, 025 (2018). arXiv:1802.05095 [gr-qc]
18. C. Bambi, L. Modesto, Rotating regular black holes. Phys. Lett. B **721**, 329–334 (2013). arXiv:1302.6075 [gr-qc]
19. B. Toshmatov, B. Ahmedov, A. Abdujabbarov, Z. Stuchlik, Rotating regular black hole solution. Phys. Rev. D **89**(10), 104017 (2014). arXiv:1404.6443 [gr-qc]
20. M.E. Rodrigues, E.L.B. Junior, G.T. Marques, V.T. Zanchin, Regular black holes in f(R) gravity coupled to nonlinear electrodynamics. Phys. Rev. D **94**(2), 024062 (2016). arXiv:1511.00569 [gr-qc]
21. M.E. Rodrigues, J.C. Fabris, E.L.B. Junior, G.T. Marques, Generalisation for regular black holes on general relativity to f(R) gravity. Eur. Phys. J. C **76**(5), 250 (2016). arXiv:1601.00471 [gr-qc]
22. M.V. de S. Silva, M.E. Rodrigues, Regular black holes in f(G) gravity. Eur. Phys. J. C **78**(8), 638 (2018). arXiv:1808.05861 [gr-qc]
23. M.E. Rodrigues, M.V. de S. Silva, Regular multi-horizon black holes in f(G) gravity with nonlinear electrodynamics. Phys. Rev. D **99**(12), 124010 (2019). arXiv:1906.06168 [gr-qc]
24. E.L.B. Junior, M.E. Rodrigues, M.V. de S. Silva, Regular black holes in rainbow gravity. Nucl. Phys. B **961**, 115244 (2020). arXiv:2002.04410 [gr-qc]
25. M.E. Rodrigues, M.V. de S. Silva, H.A. Vieira, Bardeen–Kiselev black hole with a cosmological constant. Phys. Rev. D **105**(8), 084043 (2022). https://doi.org/10.1103/PhysRevD.105.084043. arXiv:2203.04965 [gr-qc]
26. M.E. Rodrigues, H.A. Vieira, Bardeen solution with a cloud of strings. Phys. Rev. D **106**(8), 084015 (2022). https://doi.org/10.1103/PhysRevD.106.084015. arXiv:2210.06531 [gr-qc]
27. V. Bozza, Gravitational lensing in the strong field limit. Phys. Rev. D **66**, 103001 (2002). https://doi.org/10.1103/PhysRevD.66.103001. arXiv:gr-qc/0208075
28. C.F.B. Macedo, L.C.B. Crispino, Absorption of planar massless scalar waves by Bardeen regular black holes. Phys. Rev. D **90**(6), 064001 (2014). https://doi.org/10.1103/PhysRevD.90.064001. arXiv:1408.1779 [gr-qc]
29. C.F.B. Macedo, E.S. de Oliveira, L.C.B. Crispino, Scattering by regular black holes: planar massless scalar waves impinging upon a Bardeen black hole. Phys. Rev. D **92**(2), 024012 (2015). https://doi.org/10.1103/PhysRevD.92.024012. arXiv:1505.07014 [gr-qc]
30. M.A.A. Paula, L.C.S. Leite, L.C.B. Crispino, Electrically charged black holes in linear and nonlinear electrodynamics: geodesic analysis and scalar absorption. Phys. Rev. D **102**(10), 104033 (2020). https://doi.org/10.1103/PhysRevD.102.104033. arXiv:2011.08633 [gr-qc]
31. M.A.A. de Paula, L.C.S. Leite, L.C.B. Crispino, Scattering properties of charged black holes in nonlinear and Maxwell's electrodynamics. Eur. Phys. J. Plus **137**(7), 785 (2022). https://doi.org/10.1140/epjp/s13360-022-02916-z. arXiv:2207.05215 [gr-qc]

32. R. Kumar, A. Kumar, S.G. Ghosh, Testing rotating regular metrics as candidates for astrophysical black holes. Astrophys. J. **896**(1), 89 (2020). https://doi.org/10.3847/1538-4357/ab8c4a. arXiv:2006.09869 [gr-qc]
33. Z. Stuchlík, J. Schee, Shadow of the regular Bardeen black holes and comparison of the motion of photons and neutrinos. Eur. Phys. J. C **79**(1), 44 (2019). https://doi.org/10.1140/epjc/s10052-019-6543-8
34. H.C.D. Lima Junior, L.C.B. Crispino, P.V.P. Cunha, C.A.R. Herdeiro, Can different black holes cast the same shadow? Phys. Rev. D **103**(8), 084040 (2021). https://doi.org/10.1103/PhysRevD.103.084040. arXiv:2102.07034 [gr-qc]
35. I.I. Shapiro, Fourth test of general relativity. Phys. Rev. Lett. **13**, 789–791 (1964). https://doi.org/10.1103/PhysRevLett.13.789
36. R. D'Inverno, J. Vickres, *Introducing Einstein's Relativity*, 2nd edn. (Oxford University Press, Oxford, 2022)
37. C.M. Will, The confrontation between general relativity and experiment. Living Rev. Relativ. **17**, 4 (2014). https://doi.org/10.12942/lrr-2014-4. arXiv:1403.7377 [gr-qc]
38. B. Bertotti, L. Iess, P. Tortora, A test of general relativity using radio links with the Cassini spacecraft. Nature **425**, 374–376 (2003)
39. I.G. Dymnikova, Gravitational time delay of signals in the Kerr metric, in *Proceedings of the Symposium, Leningrad, USSR, May 28–31, 1985 (A87-24502 09-90)* (D. Reidel Publishing Co., Dordrecht, 1986), pp. 411–416
40. G. He, W. Lin, Second order Kerr–Newman time delay. Phys. Rev. D **93**(2), 023005 (2016). https://doi.org/10.1103/PhysRevD.93.023005. arXiv:2007.10566 [gr-qc]
41. G. He, W. Lin, Second-order time delay by a radially moving Kerr–Newman black hole. Phys. Rev. D **94**(6), 063011 (2016). https://doi.org/10.1103/PhysRevD.94.063011. arXiv:2007.11809 [gr-qc]
42. G. Feng, J. Huang, An optical perspective on the theory of relativity—II: gravitational deflection of light and Shapiro time delay. Optik (2020). https://doi.org/10.1016/j.ijleo.2020.165685
43. S.M. Kopeikin, Testing relativistic effect of propagation of gravity by very long baseline interferometry. Astrophys. J. Lett. **556**, L1–L6 (2001). https://doi.org/10.1086/322872. arXiv:gr-qc/0105060
44. S.M. Kopeikin, PostNewtonian treatment of the VLBI experiment on September 8, 2002. Phys. Lett. A **312**, 147–157 (2003). https://doi.org/10.1016/S0375-9601(03)00613-3. arXiv:gr-qc/0212121
45. S.M. Kopeikin, The measurement of the light deflection from Jupiter: theoretical interpretation. arXiv:astro-ph/0302462
46. E.B. Fomalont, S.M. Kopeikin, The measurement of the light deflection from Jupiter: experimental results. Astrophys. J. **598**, 704–711 (2003). https://doi.org/10.1086/378785. arXiv:astro-ph/0302294
47. C.M. Will, Propagation speed of gravity and the relativistic time delay. Astrophys. J. **590**, 683–690 (2003). https://doi.org/10.1086/375164. arXiv:astro-ph/0301145
48. V.M. Kaspi, J.H. Taylor, M.F. Ryba, High-precision timing of millisecond pulsars. III. Long-term monitoring of PSRs B1855+09 and B1937+21. Astrophys. J. **428**, 713 (1994). https://doi.org/10.1086/174280
49. I.H. Stairs, Z. Arzoumanian, F. Camilo, A.G. Lyne, D.J. Nice, J.H. Taylor, S.E. Thorsett, A. Wolszczan, Measurement of relativistic orbital decay in the psr b1534+12 binary system. Astrophys. J. **505**, 352 (1998). https://doi.org/10.1086/306151. arXiv:astro-ph/9712296
50. B. Ben-Salem, E. Hackmann, Propagation time delay and frame dragging effects of lightlike geodesics in the timing of a pulsar orbiting SgrA*. Mon. Not. R. Astron. Soc. **516**(2), 1768–1780 (2022). https://doi.org/10.1093/mnras/stac2337. arXiv:2203.10931 [gr-qc]
51. F. Camilo, R.S. Foster, A. Wolszczan, High-precision timing of PSR J1713+0747: Shapiro delay. Astrophys. J. Lett. **437**, L39 (1994). https://doi.org/10.1086/187677
52. E. Fonseca, H.T. Cromartie, T.T. Pennucci, P.S. Ray, A.Y. Kirichenko, S.M. Ransom, P.B. Demorest, I.H. Stairs, Z. Arzoumanian, L. Guillemot et al., Refined mass and geometric measurements of the high-mass PSR J0740+6620. Astrophys. J. Lett. **915**(1), L12 (2021). https://doi.org/10.3847/2041-8213/ac03b8. arXiv:2104.00880 [astro-ph.HE]
53. A. Hook, J. Huang, Probing axions with neutron star inspirals and other stellar processes. JHEP **06**, 036 (2018). https://doi.org/10.1007/JHEP06(2018)036. arXiv:1708.08464 [hep-ph]
54. T.K. Poddar, Constraints on axionic fuzzy dark matter from light bending and Shapiro time delay. JCAP **09**, 041 (2021). https://doi.org/10.1088/1475-7516/2021/09/041. arXiv:2104.09772 [hep-ph]
55. F.S.N. Lobo, M.E. Rodrigues, M.V. de S. Silva, A. Simpson, M. Visser, Novel black-bounce spacetimes: wormholes, regularity, energy conditions, and causal structure. Phys. Rev. D **103**(8), 084052 (2021). https://doi.org/10.1103/PhysRevD.103.084052. arXiv:2009.12057 [gr-qc]
56. S. Zhou, J. Chen, Y. Wang, Geodesic structure of test particle in Bardeen spacetime. Int. J. Mod. Phys. D **21**, 1250077 (2012). https://doi.org/10.1142/S0218271812500770. arXiv:1112.5909 [gr-qc]
57. M.F. Shamir, Massive compact Bardeen stars with conformal motion. Phys. Lett. B **811**, 135927 (2020). https://doi.org/10.1016/j.physletb.2020.135927. arXiv:2011.06932 [gr-qc]
58. A. Bhadra, K.K. Nandi, Gravitational time advancement and its possible detection. Gen. Relativ. Gravit. **42**, 293–302 (2010). https://doi.org/10.1007/s10714-009-0842-6. arXiv:0808.3729 [gr-qc]
59. X.M. Deng, Y. Xie, Gravitational time advancement under gravity's rainbow. Phys. Lett. B **772**, 152–158 (2017). https://doi.org/10.1016/j.physletb.2017.06.036
60. S. Weinberg, *Gravitation and Cosmology: Principles and Applications of the General Theory of Relativity* (Wiley, New York, 1972)
61. V.P. Frolov, A. Zelnikov, *Introduction to Black Hole Physics* (OUP, Oxford, 2011)
62. I.S. Gradshteyn, I.M. Ryzhik, *Table of Integrals, Series, and Products*, 7th edn. (Academic Press, Cambridge, 2007)
63. C.W. Chou, D.B. Hume, J.C.J. Koelemeij, D.J. Wineland, T. Rosenband, Frequency comparison of two high-accuracy Al^+ optical clocks. Phys. Rev. Lett. **104**, 070802 (2010). https://doi.org/10.1103/PhysRevLett.104.070802
64. C.W. Chou, D.B. Hume, T. Rosenband, D.J. Wineland, Optical clocks and relativity. Science **329**, 1630 (2010). https://doi.org/10.1126/science.1192720
65. W. Zhang, S.L. Bromley, J. Ye, An optical lattice clock with accuracy and stability at the 10^{-18} level. Nature **506**, 71–75 (2014). https://doi.org/10.1038/nature12941. arXiv:1309.1137
66. C. Bambi, L. Modesto, Rotating regular black holes. Phys. Lett. B **721**, 329–334 (2013). https://doi.org/10.1016/j.physletb.2013.03.025. arXiv:1302.6075 [gr-qc]
67. B. Toshmatov, B. Ahmedov, A. Abdujabbarov, Z. Stuchlik, Rotating regular black hole solution. Phys. Rev. D **89**(10), 104017 (2014). https://doi.org/10.1103/PhysRevD.89.104017. arXiv:1404.6443 [gr-qc]
68. J.C.S. Neves, A. Saa, Regular rotating black holes and the weak energy condition. Phys. Lett. B **734**, 44–48 (2014). https://doi.org/10.1016/j.physletb.2014.05.026. arXiv:1402.2694 [gr-qc]
69. S.A. Hayward, Formation and evaporation of regular black holes. Phys. Rev. Lett. **96**, 031103 (2006). https://doi.org/10.1103/PhysRevLett.96.031103. arXiv:gr-qc/0506126
70. H. Culetu, Int. J. Theor. Phys. **54**(8), 2855–2863 (2015). https://doi.org/10.1007/s10773-015-2521-6. arXiv:1408.3334 [gr-qc]